





Fragility of quantum correlations and coherence in a multipartite photonic systemHuan Cao,^{1,2,*} Chandrashekar Radhakrishnan ^{3,4,5,*} Ming Su,^{6,4} Md. Manirul Ali,⁷ Chao Zhang ^{1,2,†}
Yun-Feng Huang ^{1,2,‡} Tim Byrnes,^{3,8,4,9,10,§} Chuan-Feng Li ^{1,2,||} and Guang-Can Guo^{1,2}¹CAS Key Laboratory of Quantum Information, University of Science and Technology of China, Hefei, Anhui 230026, China²CAS Center For Excellence in Quantum Information and Quantum Physics, University of Science and Technology of China, Hefei, Anhui 230026, China³New York University Shanghai, 1555 Century Avenue, Pudong, Shanghai 200122, China⁴NYU-ECNU Institute of Physics at NYU Shanghai, 3663 Zhongshan Road North, Shanghai 200062, China⁵Laboratoire ESIEA Numérique et Société, ESIEA, 9 Rue Vesale, Paris 75005, France⁶ARC Center for Engineered Quantum Systems, School of Mathematics and Physics, University of Queensland, Brisbane, Queensland 4072, Australia⁷Department of Physics, National Cheng Kung University, Tainan 70101, Taiwan⁸State Key Laboratory of Precision Spectroscopy, School of Physical and Material Sciences, East China Normal University, Shanghai 200062, China⁹National Institute of Informatics, 2-1-2 Hitotsubashi, Chiyoda-ku, Tokyo 101-8430, Japan¹⁰Department of Physics, New York University, New York, New York 10003, USA

(Received 19 December 2019; accepted 26 May 2020; published 6 July 2020)

Certain quantum states are well known to be particularly fragile in the presence of decoherence, as illustrated by Schrödinger's famous gedanken cat experiment. More recently it has been considered that quantum states can be characterized through a hierarchy of quantum quantities such as entanglement, quantum correlations, and quantum coherence. It has been conjectured that each of these quantities has various degrees of fragility in the presence of decoherence. Here we experimentally confirm this conjecture by preparing tripartite photonic states and subjecting them to controlled amounts of dephasing. When the dephasing is applied to all the qubits, we find that the entanglement is the most fragile quantity, followed by the quantum coherence and then mutual information. This is in agreement with the widely held expectation that multipartite quantum correlations are a highly fragile manifestation of quantumness. We also perform dephasing on one of the three qubits on star and $W\bar{W}$ states. Here the distribution of the correlations and coherence in the star state becomes more important in relation to the dephasing location.

DOI: [10.1103/PhysRevA.102.012403](https://doi.org/10.1103/PhysRevA.102.012403)**I. INTRODUCTION**

One of the main challenges in the development of quantum technologies is how to overcome decoherence [1–3]. Quantum systems tend to couple very easily to their external environment, thereby losing their quantum nature and being reduced to a classical state [4,5]. It is however also well known that the timescale for which a quantum state decoheres is very much a state-dependent process. For example, superpositions of macroscopically distinct states, such as Schrödinger cat states $|0\rangle^{\otimes N} + |1\rangle^{\otimes N}$, where N is the number of qubits, collapse exponentially fast in comparison to a product state of qubits $(|0\rangle + |1\rangle)^{\otimes N}$. The fragility (or conversely the robustness) of quantum states has been studied in numerous studies [6–9]. The fragility of quantum states has been discussed in connection with measures of defining the macroscopicity of quantum

superpositions [6,10,11]. The fragility of particular quantum states can be considered the flip side of the enhanced sensitivity of such states, the classic example being NOON states, which are fundamental in the field of quantum metrology [12–14].

Meanwhile, quantum information theory has provided numerous tools in order to better understand the nature of quantum states. Various quantifiers for the strength of Bell correlations [15,16], Einstein-Podolsky-Rosen (EPR) steering [17], entanglement [18], and quantum correlations [19,20] have been proposed, each characterizing different aspects of quantum states. For example, entanglement is strictly defined as any state that is not writable in a separable form, whereas quantum correlations arise when it is impossible to disturb a quantum state with local projective measurements [19]. Recently, another quantifier, quantum coherence, has attracted attention as another way of characterizing quantum states [21]. Unlike quantum correlations that require at least bipartite systems to exist, quantum coherence can occur on a single system and is a measure of the degree of superposition [22,23]. These quantifiers form a hierarchical structure, where quantities higher in the hierarchy possess as attributes nonzero values of lower quantities [24,25]. For example, a system

*These authors contributed equally to this work.

†drzhang.chao@ustc.edu.cn

‡hyf@ustc.edu.cn

§tim.byrnes@nyu.edu

||cfli@ustc.edu.cn

possessing entanglement necessarily possesses quantum correlations and coherence, but does not necessarily show Bell correlations or steering. In particular, a unified theory connecting various types of quantum correlations was proposed by Modi *et al.* in Ref. [26]. Giorgi and Zambrini extended this approach to include various types of coherence in Ref. [27]. Various quantum technological tasks rely on different properties of quantum states; hence one of the major aims of quantum information theory is to understand the operational capability of these different resources [28–34]. How these resources behave in a dynamical context has been a focus of several works [35–38], motivated by the presence of environmental decoherence in quantum technological systems.

In this study we experimentally show the effect of the different quantum correlations and coherences of a tripartite photonic system under the influence of a one- and a three-qubit dephasing environment. We compute the six quantities, (i) entanglement, (ii) total coherence, (iii) global coherence, (iv) local coherence, (v) mutual information, and (vi) classical correlations, and measure their decay dynamics under dephasing. The above quantities are computed from the tomographic reconstruction of the density matrices corresponding to the experimentally generated quantum state. The fragility of these quantities under dephasing is investigated by measuring the decay rate, which can quantify the fragility of the quantity under question. We note that investigations on the transient dynamics of entanglement and quantum discord have been performed in Refs. [35–45]. Particularly in Refs. [35–38], an experimental verification of the decay dynamics has been examined. In our work we focus on studying the *comparative* dephasing dynamics of different quantum properties using relative entropy measures. To observe the decay dynamics of multipartite quantum states, we generate the $W\bar{W}$ and star states, which contain correlations and coherences at all levels. Such states are uniquely suited for examining multiple quantum properties simultaneously.

In Sec. II we discuss the two quantum states under investigation and their experimental preparation. The various measures of correlations and coherence are explained in Sec. III. The evolution of the density matrix under dephasing is described in Sec. IV within the two main topics of tomographic reconstruction of states and decay of correlations and coherence under dephasing. In Sec. V we present a summary and our conclusions.

II. PHOTONIC STATE GENERATION

A. $W\bar{W}$ and star states

In this study we generate and study the dynamics of two quantum states under dephasing. The first state is the $W\bar{W}$ state defined as

$$|W\bar{W}\rangle = \frac{1}{\sqrt{2}}(|W\rangle + |\bar{W}\rangle), \quad (1)$$

$$|W\rangle = \frac{1}{\sqrt{3}}(|001\rangle + |010\rangle + |100\rangle), \quad (2)$$

$$|\bar{W}\rangle = \frac{1}{\sqrt{3}}(|110\rangle + |101\rangle + |011\rangle). \quad (3)$$

The $W\bar{W}$ state is an equal superposition of a standard W state and its spin-flipped version, the \bar{W} state. This type of state is chosen because it has quantum coherence at the single-qubit,

bipartite, and tripartite levels, as well as bipartite and tripartite quantum correlations. Such a state is a good test bed for studying quantum correlations distributed at different levels. The presence of different types of correlations is one of the reasons that W states are robust under local decoherence [46].

The second state we investigate is the star state defined as

$$|S\rangle = \frac{1}{2}(|000\rangle + |100\rangle + |101\rangle + |111\rangle). \quad (4)$$

Like the $W\bar{W}$ state, the star state also has coherence and correlations distributed at all possible levels. However, the correlations are present in an asymmetric way for a star state, in contrast to the $W\bar{W}$ state, which is symmetric for all qubits. The entanglement structure for the star state takes the form $A \Leftrightarrow C \Leftrightarrow B$, where we have labeled the three qubits as ABC in (4) from left to right. For example, if qubit A or B is traced out, entanglement is present in the remaining qubits. However, if qubit C is traced out, the remaining qubits are left in a separable state. We thus call qubit C the central qubit and qubits A and B are the peripheral qubits. The star state is a very simple example of a graph state [47], which in multipartite cases is useful for quantum error correction [48]. More details on the distribution of correlations and coherence in the $W\bar{W}$ and star states are given in Appendix B.

B. Experimental preparation

To experimentally realize the above states, polarization encoded photonic qubits are used, where the horizontal (H) and vertical (V) polarizations are encoded as the two levels $|0\rangle$ and $|1\rangle$, respectively. The detailed procedure of preparing these quantum states is shown in Fig. 1. In our experiment we investigate the dynamics of various correlations and coherence in a tripartite quantum system which is under the influence of an external phase damping environment, realized by passing the photonic states through birefringent quartz crystals of different thicknesses. We perform two types of dephasing, where all three photons are dephased by a crystal of the same thickness, and another where only one of the photons is dephased. The dephasing on only one of the photons allows for a partial dephasing of the system, where some quantum property is retained even after complete dephasing.

The experimental setup to prepare the $W\bar{W}$ is shown in Fig. 1(a). Two pairs of down-converted photons are simultaneously generated through a higher-order emission of the spontaneous parametric down-conversion (SPDC) process. These four photons are collected by a single-mode fiber and then fed into a polarizing beam splitter (PBS) where they overlap and become indistinguishable in the spatial mode. The spectral selection is realized by inserting a 3-nm interference filter after the PBS. The four photons are separated by three nonpolarizing beam splitters. The postselected fourfold coincidence count certifies the generation of a four-photon Dicke state with two excitations $|D_4^2\rangle = (|0011\rangle + |0101\rangle + |1001\rangle + |0110\rangle + |1010\rangle + |1100\rangle)/\sqrt{6}$. The $W\bar{W}$ state is generated from the Dicke state by projecting one of the qubits into the $(|0\rangle + |1\rangle)/\sqrt{2}$ basis.

The star state generation scheme is shown in Fig. 1(b). Two nonmaximally entangled bipartite states $|\psi\rangle = \cos\theta|01\rangle + \sin\theta|10\rangle$ with the ratio $\cos^2\theta : \sin^2\theta = 6.8554$ are required to prepare the star state. These polarization entangled states

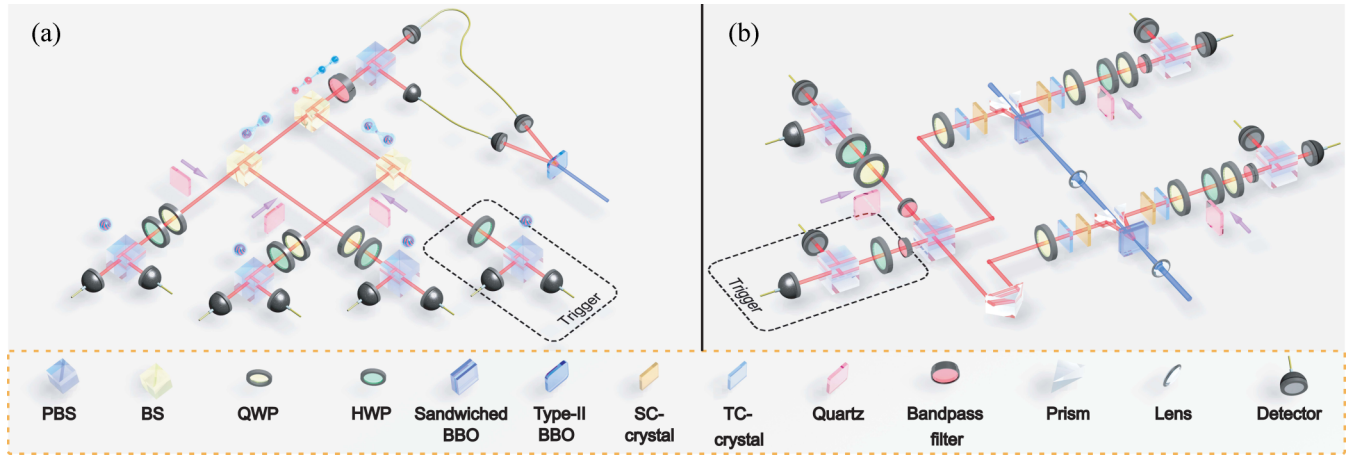


FIG. 1. Experimental setup for the preparation, dephasing, and measurement of the (a) $W\bar{W}$ state and (b) star state. In (a) the down-converted photons are collected by a single fiber coupler. The output coupler before the first polarizing beam splitter (PBS) is mounted on a translational stage to make fine adjustments with the arrival time of the photons. Each beam splitter (BS) consists of one 0° plate BS and a 45° mirror in its reflection path. The mirror introduces a phase shift of π between $|H\rangle$ and $|V\rangle$ which is to compensate the phase shift introduced by the BS. Such a setup makes the reflectivity more polarization independent than a cube BS. Since this requires no phase modulation the setup can be stable over several days. The final triggered photon is detected using a half waveplate (HWP), a PBS, and a detector. Each photon of a $W\bar{W}$ state is analyzed using a polarization measurement system consisting of a quarter waveplate (QWP), HWP, PBS, and two fiber-coupled single-photon detectors. (b) In each arm of the EPR pairs, one crystal is used for temporal compensation (TC) and one crystal is used for spatial compensation (SC), through which the two possible ways of generating photon pairs (first or second crystal in sandwiched BBO) are made indistinguishable. The two extraordinarily down-converted photons produced by the cascaded sandwich beam source are superposed on a PBS. The time of arrival of photons is adjusted with prisms. Further details on the experiment can be seen in the Appendices.

are generated using a sandwiched geometry beamlike type-II β barium borate (BBO) entanglement resource. Such an entanglement resource was first devised by Zhang *et al.* in Ref. [49] and was later used in Ref. [50] to realize ten-photon entanglement. Applying single-qubit unitary operators on each qubit, the state $|\psi\rangle$ is transformed to $(|00\rangle + |10\rangle + |11\rangle)/\sqrt{3}$. The transformed states are fed into the PBS to overlap them and the Hong-Ou-Mandel interference visibility is enhanced using a 2-nm bandpass filter. The second of the four-qubit quantum states generated through this process is projected in the $(|0\rangle + |1\rangle)/\sqrt{2}$ basis. By exchanging qubits 3 and 4 in the resulting quantum state, the star states are obtained.

III. MEASURES OF CORRELATIONS AND COHERENCE

We measure the correlations and coherence using the unified distance-based approach of Ref. [26]. The basic idea of any distance-based approach to quantify a quantum observable is as follows. First the set of all states that do not have the relevant quantity is defined and the states are called reference states. For example, for entanglement, the reference states are the set of all separable states. Then, to quantify the quantum property, one uses a suitable distance measure to find the distance to the closest reference state by minimization. In our case, we choose the distance measure to be relative entropy

$$S(\rho\|\sigma) = \text{Tr}(\rho \ln \rho - \rho \ln \sigma), \quad (5)$$

where ρ is the quantum state in which correlations are measured and σ is the reference quantum state which does not possess the quantum property. This measure is a popular choice due to its simplicity of computation and well-known

properties [51]. The six quantities that we calculate are defined below and are summarized in Table I.

Entanglement. The entanglement is quantified as the minimum distance to the set of all separable states [52,53]. We perform a minimization procedure to separable states taking the form $\sum_j p_j \rho_j^A \otimes \rho_j^B \otimes \rho_j^C$, where p_j is a probability and $\rho_j^{A,B,C}$ are density matrices on subsystems A , B , and C .

Coherence. The total quantum coherence [21] is defined as the distance to the closest incoherent state, which takes the form $\sum_j p_j |j\rangle\langle j|$, where $|j\rangle$ is in the basis $\{|0\rangle, |1\rangle\}$ for A , B , and C . It has been shown that for the relative entropy, the closest incoherent state to a state ρ takes coefficients $p_j = \langle j|\rho|j\rangle$; hence the minimization does not need to be explicitly performed [21] and

$$C(\rho) = \min_{\sigma \in \mathcal{I}} S(\rho\|\sigma) = S(\rho\|\rho_d) = S(\rho_d) - S(\rho). \quad (6)$$

Here we define ρ_d as the matrix ρ with all off-diagonal terms set to zero in the basis $|j\rangle$.

Local and global coherence. Quantum coherence can originate from coherence which is localized on subsystems or coherence due to a collective property of the whole system [22,23]. The former is called local coherence and is found by first breaking all the correlations between the subsystems. In a similar way to total coherence, the closest incoherent state is found by taking the diagonal form

$$C_L(\rho) = \min_{\sigma \in \mathcal{I}} S(\pi(\rho)\|\sigma) = S(\pi(\rho)\|\pi_d(\rho)), \quad (7)$$

where $\pi(\rho) = \rho_A \otimes \rho_B \otimes \rho_C$ is the product density matrix with $\rho_A = \text{Tr}_{BC} \rho_{ABC}$ the single-qubit reduced density matrix and $\pi_d(\rho)$ the matrix $\pi(\rho)$ but with all off-diagonal elements set to zero in the basis $|j\rangle$. The coherence attributed to the

TABLE I. List of properties of a quantum state ρ and their measurement procedure.

Quantity	Reference state	Example reference state σ	Definition
entanglement	separable state \mathcal{S}	$\sum_j p_j \rho_j^A \otimes \rho_j^B \otimes \rho_j^C$	$E = \min_{\sigma \in \mathcal{S}} S(\rho \parallel \sigma)$
total coherence	incoherent state \mathcal{I}	$\rho_d = \sum_j \langle j \rho j \rangle j\rangle \langle j $	$C = \min_{\sigma \in \mathcal{I}} S(\rho \parallel \sigma)$
local coherence	incoherent states $\bar{\mathcal{I}}$	$\pi_d(\rho) = \rho_d^A \otimes \rho_d^B \otimes \rho_d^C$	$C_L = \min_{\pi(\rho) \in \bar{\mathcal{I}}} S(\pi(\rho) \parallel \sigma)$
mutual information (total correlations)	product state \mathcal{P}	$\pi(\rho) = \rho^A \otimes \rho^B \otimes \rho^C$	$T = \min_{\sigma \in \mathcal{P}} S(\rho \parallel \sigma)$
classical correlation	product state \mathcal{P}	$\pi(\rho_d)$	$K = \min_{\sigma \in \mathcal{P}} S(\rho_d \parallel \sigma)$
hookup	incoherent product states $\bar{\mathcal{I}}$	$\pi_d(\rho) = \pi(\rho_d)$	$M = \min_{\sigma \in \bar{\mathcal{I}}} S(\rho \parallel \sigma)$

collective nature of the system is called global coherence and is defined as the difference of the total and local coherence

$$C_G(\rho) = C(\rho) - C_L(\rho). \quad (8)$$

Mutual information. Mutual information measures the total amount of correlation, including both quantum and classical parts [26]. The set of uncorrelated states takes the form of a product state $\sigma^A \otimes \sigma^B \otimes \sigma^C$. It has been shown in Ref. [26] that for relative entropy the closest product state is the product state $\pi(\rho) = \rho^A \otimes \rho^B \otimes \rho^C$ consisting of the reduced density matrices on each subsystem $\rho^{A,B,C}$. Hence we can write

$$T(\rho) = \min_{\sigma \in \mathcal{P}} S(\rho \parallel \sigma) = S(\rho \parallel \pi(\rho)) \equiv S(\pi(\rho)) - S(\rho). \quad (9)$$

The total correlations as measured by the mutual information T and the total quantum coherence C are not completely independent quantities. Hence there is a common region of quantumness in a system which is measured by both these quantities. This region of overlap is the amount of global coherence in the system which arises due to quantum correlations between the qubits.

Classical correlations. For local coherence, first the correlations between the subsystems are broken and then the remaining coherence is measured. The reverse ordering can equally be performed, where first the coherence is removed from the system and then the remaining correlations are measured. The state with no coherence is ρ_d , which can only contain classical correlations because it is a diagonal density matrix [27]. In the same way as for mutual information, the closest uncorrelated state is its corresponding product state

$$K(\rho) = \min_{\sigma \in \mathcal{P}} S(\rho_d \parallel \sigma) = S(\rho_d \parallel \pi(\rho_d)). \quad (10)$$

Hookup. The reference state for total coherence C is ρ_d , which is a state that has no coherence but potentially classical correlations. Meanwhile, the reference state for the mutual information T is $\pi(\rho)$, which has no correlations but potentially coherence. One can define a quantity with a reference state that has no correlations and no coherence. This was called the hookup in Ref. [27] and can be evaluated to be

$$M(\rho) = C(\rho) + K(\rho) = T(\rho) + C_L(\rho). \quad (11)$$

Of the different measured quantities, entanglement, total coherence, local coherence, and global coherence measure purely quantum properties. The entanglement is a measure of the nonseparability of quantum states, the global coherence is the coherence attributed to the collective quantum states, and the local coherence estimates the quantumness localized

in the qubit. The total coherence, which is the sum of the local and global coherence, estimates the total quantumness in the system. The mutual information and hookup measure features which are partly quantum and partly classical by nature. Finally, as the name suggests, the classical correlations are correlations that are in the incoherent basis (i.e., $|0\rangle$ and $|1\rangle$). A detailed overview of the various correlations and coherence is given in Appendix A.

IV. DENSITY-MATRIX EVOLUTION UNDER DEPHASING

A. Tomography reconstruction of states

Figure 2 shows the tomographic reconstructions of the star and $W\bar{W}$ states with various amounts of dephasing. For the case where the dephasing is applied to all the photons, the density matrix approaches its diagonal form as expected for larger values of ℓ , the thickness of the quartz plate. In the case where dephasing is only applied to one of the photons, some of the off-diagonal terms remain since the state is only partially dephased. This is due to the nature of the star and $W\bar{W}$ states that are used which contain types of coherence other than completely tripartite coherence [such as in a Greenberger-Horne-Zeilinger (GHZ) state]. The tomographically reconstructed density matrix is compared to the theoretically calculated density matrix according to a dephasing channel for each qubit defined as

$$\rho \rightarrow [1 - p(\ell)]\rho + p(\ell)\sigma_z\rho\sigma_z, \quad (12)$$

where $p(\ell) = [1 - \exp(-\Gamma\ell^2)]/2$ (see Appendix D). We obtain fidelities of the state with dephasing better than 93% for all dephasing values.

B. Decay of correlations and coherence with dephasing on all qubits

Using the tomographically reconstructed density matrices, we calculate the various quantities summarized in Table I. First we discuss the dephasing dynamics of the correlations in a $W\bar{W}$ state, as shown in Figs. 3(a) and 3(b). We observe that all quantities decay to zero for large dephasing, except the mutual information T and classical correlations K , which saturate to finite values. This is due to the dephasing removing all coherence from the system such that the state

$$\begin{aligned} \rho_d = & \frac{1}{6}(|001\rangle\langle 001| + |010\rangle\langle 010| + |100\rangle\langle 100| \\ & + |110\rangle\langle 110| + |101\rangle\langle 101| + |011\rangle\langle 011|) \end{aligned} \quad (13)$$

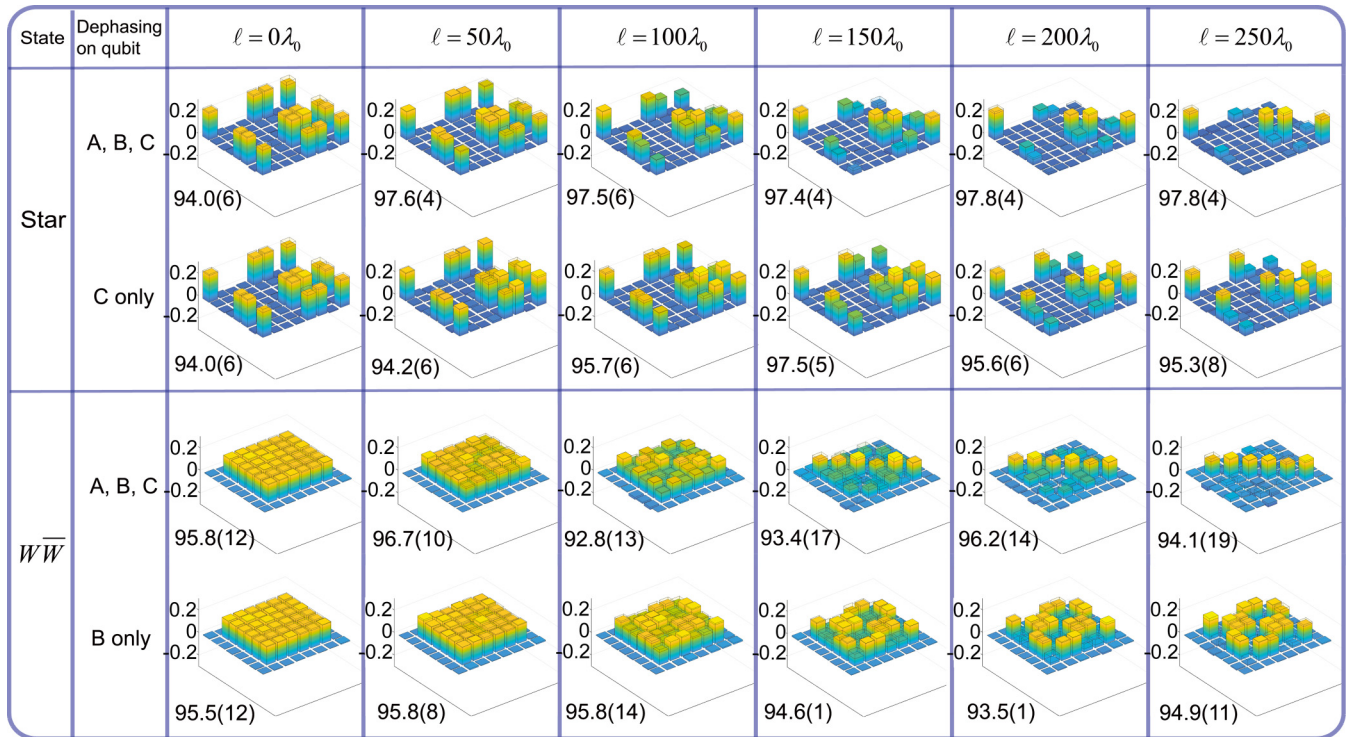


FIG. 2. Tomographic reconstruction of the density matrices of the star and $\overline{W\overline{W}}$ states for various thicknesses of quartz plates. The amount of dephasing is controlled by the quartz plate thickness ℓ . Only the real part of the density matrix elements are shown, and the imaginary parts are consistent with zero for all thicknesses (see the Appendices). The theoretical density matrix for each dephasing time is shown as a transparent histogram, and the fidelities are marked as a percentage, along with the error estimate. Dephasing rates of $\Gamma = 2.21 \times 10^{-5}\lambda_0^{-2}$ for the $\overline{W\overline{W}}$ states and $\Gamma = 2.06 \times 10^{-5}\lambda_0^{-2}$ for star states are used, with $\lambda_0 = 780$ nm.

is progressively approached. This is a classically correlated state and hence the mutual information only contains classical correlations $T = K$ is observed and all other quantum properties decay to zero. In Fig. 3(b) we see that the global coherence starts at a larger value than the local coherence, but the global coherence decays faster than the local coherence. This is an indication of the greater robustness of the local coherence in the presence of dephasing than global coherence.

To examine this point in more detail, we plot the decay rates for the various quantities in Fig. 3(c). Due to the Gaussian nature of the dephasing channel (12), we expect the quantum properties to also approximately follow a Gaussian form proportional to $\exp(-\Gamma\ell^2)$; hence the decay rate is the negative gradient on a semilogarithmic plot with ℓ^2 . Of all the quantum properties the fastest decay is for entanglement. The next fastest decay rate is displayed by global quantum coherence, followed by the total coherence. The very slow decay of mutual information is because it is composed of both quantum correlations and classical correlations. While quantum correlations decay due to the environment, the classical correlations remain unchanged, since the dephasing acts in the classical basis $|0\rangle, |1\rangle$. Likewise, local coherence can be seen to decay more slowly than the total coherence. These results generally show that the quantities that are related to collective effects, such as entanglement and global coherence, tend to decay at a faster rate than classical or local quantities.

The star state generally shows similar behavior, as can be seen in Figs. 3(d) and 3(e). Here again the mutual information and classical correlations saturate towards a nonzero value,

according to the classical correlations in the state

$$\rho_d = \frac{1}{4}(|000\rangle\langle 000| + |100\rangle\langle 100| + |101\rangle\langle 101| + |111\rangle\langle 111|). \quad (14)$$

All other quantities decay to zero, in a similar way to the $\overline{W\overline{W}}$ state. The total coherence is less in the star state due to the smaller number of terms in the superposition. Nevertheless, as seen by evaluating the decay rates in Fig. 3(f), the entanglement shows the greatest rate of decrease, followed by the global and total coherences. The mutual information and local coherences decay with the slowest rates, similar to the $\overline{W\overline{W}}$ state. Thus, despite the rather different structure of the states, a consistent picture emerges once the decay rates are examined.

C. Decay of correlations and coherence with one-qubit dephasing

One way of understanding the faster decay of the collective quantities such as entanglement and global coherence is that they are exposed to the dephasing effects from multiple qubits. This is in contrast to quantities that are localized on each qubit, such as local coherence, which can only affect one qubit at a time. In this picture, if the dephasing is only applied to one qubit, then we might expect that the rates for all quantities will be more similar. To test this hypothesis, we also perform dephasing on one qubit and investigate its effect on the various quantities as before.

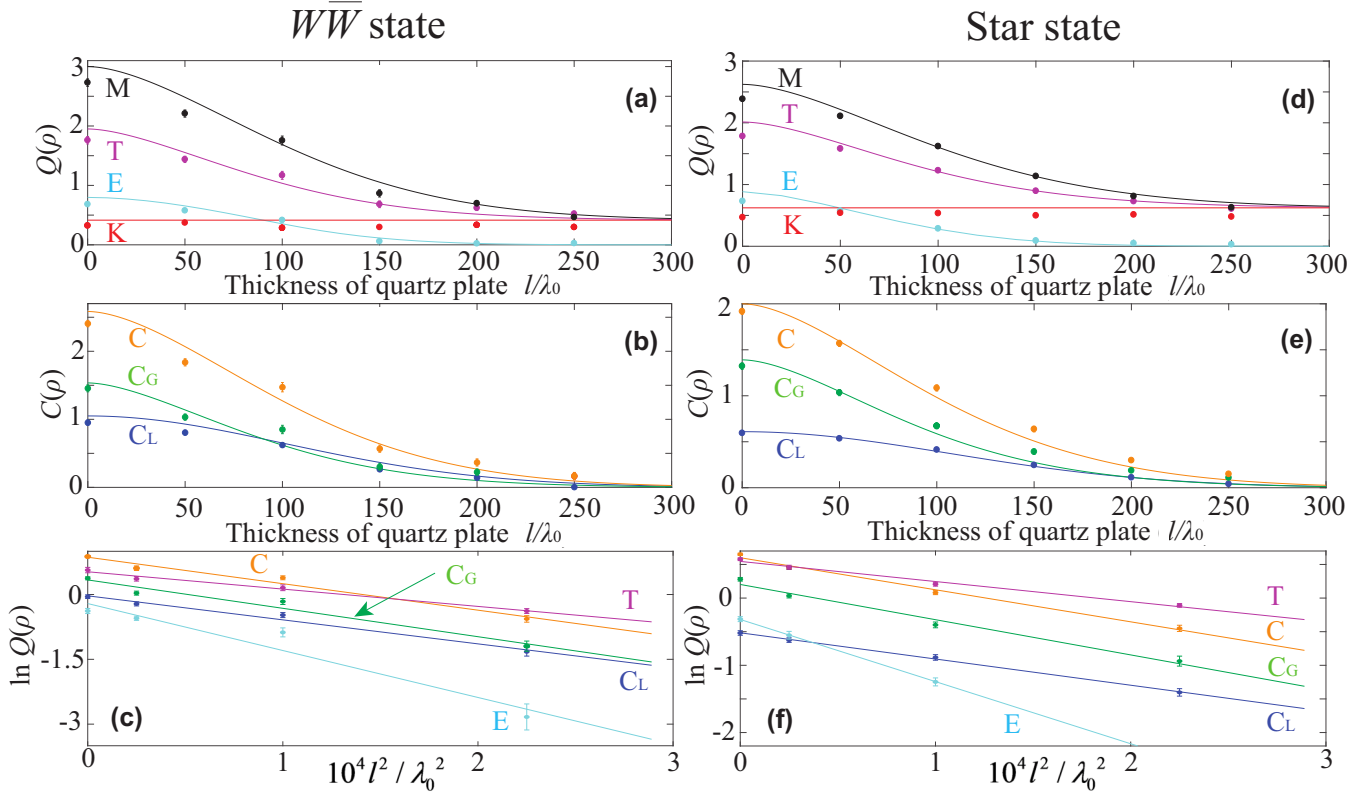


FIG. 3. Decay of quantum properties for the (a)–(c) $W\bar{W}$ and (d)–(f) star states under three-qubit dephasing. The various quantum properties are mutual information T , total coherence C , global coherence C_G , local coherence C_L , entanglement E , and classical correlations K . In (a), (b), (d), and (e) the exponential decay of these properties is shown as a function of the thickness of the quartz plate ℓ (units of $\lambda_0 = 780$ nm). Theoretical predictions are shown with the solid lines. Replotted in (c) and (f) are the same curves on a semilogarithmic plot with the x axis representing the square of the thickness of the quartz plate and the physical properties along the y axis. The slope of the linear fit gives the decay rate of the quantum property. In all panels the experimental data are denoted by points and the error bar is obtained through a simulation of the photon statistics. In (a), (b), (d), and (e) solid lines are the theoretical predictions, while in (c) and (f) the solid lines are fits to the experimental data. Fitted values of the decay rates (in units of $10^{-5}\lambda_0^{-2}$) are (c) $\Gamma(E) = 10.9$, $\Gamma(C_G) = 6.6$, $\Gamma(C) = 6.1$, $\Gamma(C_L) = 5.6$, and $\Gamma(T) = 4.0$ and (f) $\Gamma(E) = 9.2$, $\Gamma(C_G) = 5.2$, $\Gamma(C) = 4.8$, $\Gamma(C_L) = 3.9$, and $\Gamma(T) = 3.0$.

The decay of various quantities for the $W\bar{W}$ due to dephasing is shown in Figs. 4(a) and 4(b). Due to the symmetric nature of the state, dephasing any one of the three qubits leads to the same result; hence in our case qubit B is dephased. In this case all quantities saturate to a nonzero value, which is characteristic of the $W\bar{W}$ state. As is well known, dephasing of a W state only partially removes the entanglement from the system and the remaining qubits are partially entangled. This means that both quantum correlations and coherence are preserved in the system. Due to the quantum correlations that are preserved in this case, we observe that the amounts of correlation and coherence are always larger than the amount of classical correlations, in contrast to the three-qubit dephasing case.

The entanglement structure of the state plays a more important role in the case of star states, as seen in Figs. 4(d) and 4(e) for the central qubit dephasing and Figs. 4(g) and 4(i) for the peripheral dephasing. For the star state we show the effects of dephasing on the central qubit C as well as the peripheral qubit B . In this case we observe the entanglement decaying to zero for large dephasing, as expected from the discussion surrounding Eq. (4). For dephasing on a peripheral

qubit, we find that the entanglement does not decay to zero, in a similar way to the $W\bar{W}$ state (see Appendix B). Other quantities saturate to nonzero values, with the steady-state value of the global coherence being higher than the amount of classical correlations in the system. This is in contrast to the entanglement and local coherence in which the steady-state value is lower than the classical correlations. We note that compared to the other quantities the local coherence exhibits very minimal evolution due to dephasing.

Figures 4(c), 4(f), and 4(i) show a comparison of the decay rates of the various quantities, which appear as the negative gradient on the semilogarithmic plot. We find that the ordering of the decay rates does not occur in a consistent order as before. For the $W\bar{W}$ state, we find that all quantities generally decay with a similar rate, with the global coherence giving the largest value. On the other hand, for the star state, we clearly see that the entanglement decays at the fastest rate, in a similar way to the three-qubit dephasing case. We attribute this to the different structure of entanglement that is present in the two states. For the $W\bar{W}$ state, all the qubits can be considered “peripheral” qubits, since the dephasing causes only partial loss of entanglement. In the case of dephasing the central qubit of the star state, the destruction of entanglement is effective,

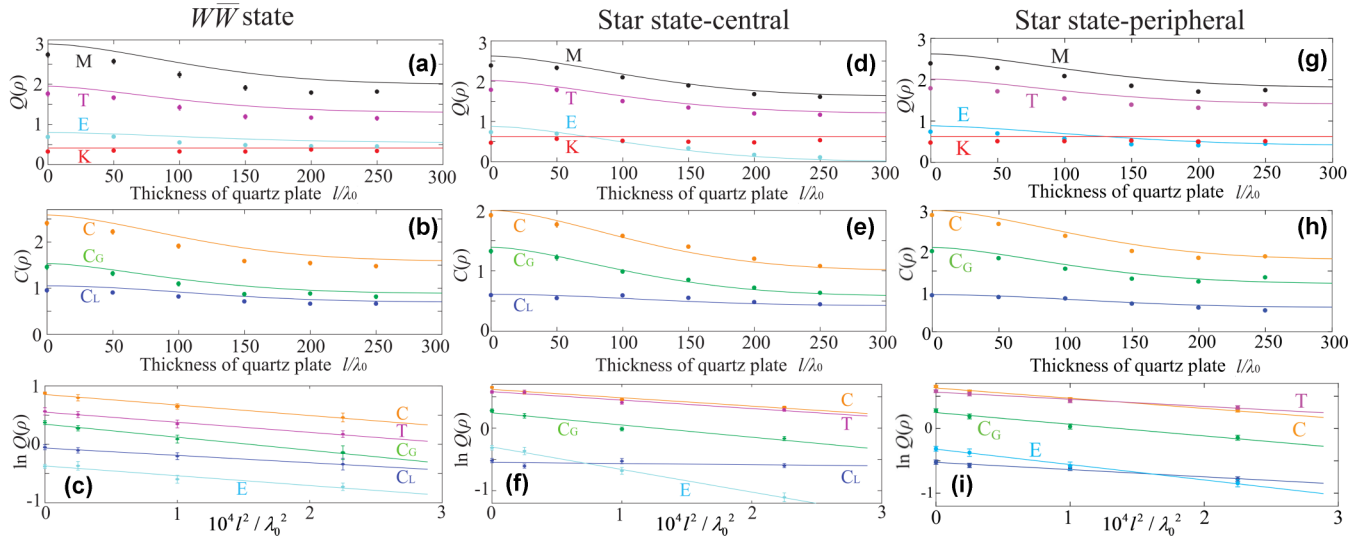


FIG. 4. Decay of quantum properties of the (a)–(c) $W\bar{W}$ and (d)–(f) star states with qubit C (central qubit) dephased and the (g)–(i) star state with qubit B (peripheral qubit) dephased. For the $W\bar{W}$ state, qubit B is dephased, while for the star state qubit C is dephased for central qubit dephasing and qubit B dephased for peripheral qubit dephasing. The labeling is the same as in Fig. 3. Points are experimental data and the lines are theoretical predictions in (a), (b), (d), (e), (g), and (h). In (c), (f), and (i) the lines are fits to the data. Fitted values of the decay rates (in units of $10^{-5}\lambda_0^{-2}$) are (c) $\Gamma(C_G) = 2.2$, $\Gamma(C) = 1.8$, $\Gamma(T) = 1.7$, $\Gamma(E) = 1.7$, and $\Gamma(C_L) = 1.3$; (f) $\Gamma(E) = 3.6$, $\Gamma(C_G) = 2.0$, $\Gamma(C) = 1.3$, $\Gamma(T) = 1.3$, and $\Gamma(C_L) = 0.2$; and (i) $\Gamma(E) = 2.4$, $\Gamma(C_G) = 1.8$, $\Gamma(C) = 1.6$, $\Gamma(T) = 1.1$, and $\Gamma(C_L) = 1.1$.

since the central qubit is individually entangled to qubits A and qubit B , which are not entangled with each other. So a dephasing of qubit C will destroy all the entanglement in the system. Thus, in this case we observe that the structure of the quantum correlations greatly affects the fragility of the state.

V. SUMMARY AND CONCLUSIONS

The dephasing effects on quantum correlations and quantum coherence were experimentally studied for photonic $W\bar{W}$ and star states. In our experiment we considered both one-qubit dephasing and three-qubit dephasing of the tripartite quantum states. Such states have coherence and correlations of all types in a tripartite system. Using a Gaussian dephasing model, we were able to extract the effective decay rates for each state and each type of dephasing, as shown in Figs. 3(c), 3(f), 4(c), and 4(f). In the case that dephasing was applied on all the qubits, a consistent picture emerged, despite the different nature of the states. Here we found that

$$\Gamma(E) > \Gamma(C_G) > \Gamma(C) > \Gamma(C_L) > \Gamma(T) > \Gamma(K), \quad (15)$$

i.e., the dephasing rates occurred in the order of entanglement, global coherence, total coherence, local coherence, mutual information, and classical correlations. We thus saw a clear hierarchy in the decay rate of the various quantum properties, where the collective quantities decayed at a faster rate than local and classical quantities. This can be understood as the result of collective quantities being affected by all the channels of dephasing, but local quantities only are affected by their local dephaser. In this way we verified the conjecture that collective quantities are more fragile than the local quantities, when local decoherence is applied on the whole system. For the case that only one qubit is dephased, the rates of decay depend more on the structure of the quantum state. In the case of dephasing the central qubit of a star state, we

again recovered the entanglement as the most fragile quantity. However, in the case of dephasing a peripheral qubit where entanglement can be retained in the strong dephasing limit, the rate of decay is much lower. Similar results were obtained theoretically in different models of dephasing [54].

The information-theoretic quantities like entanglement, mutual information, total coherence, local coherence, and global coherence are manifestations of some basic physical features. For example, entanglement is a manifestation of the nonseparability of quantum states, total quantum correlation is the interqubit quantum correlation, and local coherence is a physical feature arising due to local superposition. From the decay rate hierarchy of the information-theoretic quantities in Eq. (15), we can get the robustness hierarchy of the different quantum features as

$$DQC < TQC < LS, \quad (16)$$

where DQC, TQC, and LS stand for distributed quantum correlation, total quantum correlation, and local superposition, respectively, and the notation $A < B$ denotes that A decays faster than B . The DQC unique to quantum systems and TQC (both nonlocal and local quantum correlations) are interqubit correlations distributed between the qubits. Here LS is the superposition between the levels of a qubit and hence is an intraqubit property which is localized within a qubit. Hence we find that the interqubit quantum properties which are spread out between the qubits are more likely to decay much faster when compared to the intraqubit quantum properties, which are relatively more robust. This suggests that in quantum information-theoretic tasks it would be advantageous to use intraqubit quantum properties as resources as they can be preserved over longer time intervals. By converting between local coherence to global coherence only when it is needed [55], this could be used as a strategy for preserving coherence to longer times.

We note that in our approach the classical correlations are constant throughout the entire process of evolution. This is in contrast to the theoretical results observed in Refs. [45,56] and was subsequently experimentally examined [36]. The difference here originates from the different notions of classicality as defined by quantum discord and quantum coherence. In quantum discord, a state is classically correlated if there exist a local measurement and a conditioned measurement, in any basis, which do not disturb the quantum state [19,57]. It is therefore a quantity that is invariant under local basis transformations. In contrast, coherence is a basis-dependent quantity [58]. The classical nature of the state is with respect to a particular basis choice, in our case the $|0\rangle, |1\rangle$ basis. Here our notion of classical correlations is in this fixed basis choice, and the dephasing removes coherence in this basis. This means that the classical correlations are always unchanged under this evolution. In the case of Refs. [36,45,56], classical correlations can be dynamic because of the local basis optimization that is performed in evaluating the discord. In our view, these results are not inconsistent, but arise from different notions of classicality. In our approach, there is a preferred classical basis $|0\rangle, |1\rangle$, which is natural to consider since this is the basis that dephasing occurs in the system.

Another observation that can be made from Figs. 3 and 4 is that the amount of total quantum coherence is always higher than the entanglement present in the system. This is because the coherence originates due to collective quantum correlations, local quantum correlations, and local superpositions, whereas the entanglement arises only due to the nonlocal quantum correlations. This enables us to verify the theorem $E(\rho) \leq C(\rho)$ in Ref. [59] in a dynamical scenario, when they are both measured using the same contractive distance. This relationship between entanglement and coherence was proved in Ref. [59] under the condition that both these quantities are measured using the same contractive distance. In our work we also use the same contractive distance (relative entropy) and also verify that the relation holds under dephasing dynamics as well.

Our work demonstrates that various quantum information quantities can be used to effectively characterize quantum systems. These can be extended to larger quantum systems, where more dramatic phase transition phenomena can be observed [31]. Adding decoherence and observing the dynamics can be a direct quantifier for the fragility of various quantities. Since particular quantities are more relevant for a given quantum information task, this general method may find also practical uses in the context of applications to quantum technology.

ACKNOWLEDGMENTS

The work of C.R. and T.B. was supported by the Shanghai Research Challenge Fund, New York University Global Seed Grants for Collaborative Research, National Natural Science Foundation of China (Grants No. 61571301 and No. D1210036A), the NSFC Research Fund for International Young Scientists (Grants No. 11650110425 and No. 11850410426), NYU-ECNU Institute of Physics at NYU Shanghai, the Science and Technology Commission of Shanghai Municipality (Grant No. 17ZR1443600), the China

Science and Technology Exchange Center (Grant No. NGA-16-001), and the NSFC-RFBR Collaborative grant (Grant No. 81811530112). The work of H.C., C.Z., and Y.F.H. was supported by China Postdoctoral Science Foundation (Grant No. 2017M612074), the National Natural Science Foundation of China (Grant No. 11704371), National Natural Science Foundation of China (Grant No. 11734015), and Anhui Initiative in Quantum Information Technologies (Grant No. AHY070000).

APPENDIX A: QUANTUM PROPERTIES AND THEIR MEASUREMENT

In information-theoretic applications an important task is to compare two probability distributions $P = \{p_1, \dots, p_m\}$ and $Q = \{q_1, \dots, q_m\}$. Fundamentally there are two different methods to compare the distributions. The first method is to use the normed distance between these two distributions, for example, the ℓ_n -norm between two distributions is

$$\mathcal{D}_{\ell_n} = \left(\sum_{i=1}^m |p_i - q_i|^n \right)^{1/n}. \quad (A1)$$

For $n = 1$ we have the ℓ_1 -norm and for $n = 2$ it is the well-known Euclidean norm. The second method is to use a contrast function which compares the information between two distributions. A commonly used function in this regard, the relative entropy

$$S(P\|Q) = \sum_{i=1}^m p_i \ln \frac{p_i}{q_i} \quad (A2)$$

estimates the difference in entropy between the two distributions. In the quantum case similar comparisons are made between two density matrices $\rho, \sigma \in \mathcal{B}(\mathcal{H}_1^+)$. The relative entropy between two different density matrices is defined as

$$S(\rho\|\sigma) = \text{Tr}(\rho \ln \rho - \rho \ln \sigma). \quad (A3)$$

One can use this expression to measure the amount of quantum correlation. To do so we must consider one of the density matrices σ to be the reference state. A reference state is a very particular type of state which does not have any of the quantum correlation which is being measured. In the quantum domain one typically has a set of reference states which do not have any quantum correlations. Under such a circumstance, we usually compute the distance to the closest state in the set. This translates to finding the minimum distance of a quantum state to a set of reference states. So using the expression for the relative entropy and minimizing over the appropriate set of reference states, one can measure the amount of a given quantum correlation according to

$$\mathcal{Q} = \min_{\sigma \in \mathcal{R}} S(\rho\|\sigma). \quad (A4)$$

Here \mathcal{Q} is the quantum property and \mathcal{R} is the set of reference states. In Table I we give a list of correlations and quantum properties and their estimation procedure.

As shown in Table I, there are several measurable properties in a quantum system, but some of them have an overlap in what they measure. It is then essential to come up with a quantity which measures the complete information without

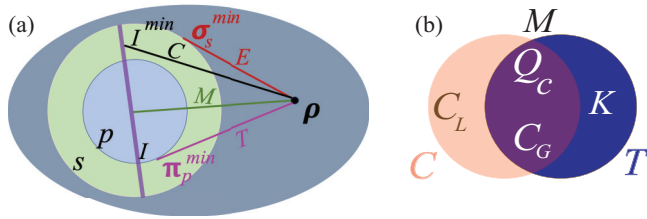


FIG. 5. (a) Definition of various properties of a quantum system as the distance between the states. Here s is the set of separable states, p is the set of product states, and \mathcal{T} is the set of incoherent states. The closest separable state, product state, and incoherent state are represented by σ_s^{\min} , π_p^{\min} , and \mathcal{I}^{\min} , respectively. (b) Unified framework for combining coherence and mutual information. The total amount of information in the system, known as the hookup M , is divided into two circular regions, namely, the coherence C and mutual information T . The overlap of the two circles denotes the quantum correlations as well as the global coherence. The classical correlations K and the local coherence C_L are the nonoverlapping regions of the mutual information and coherence.

redundancy. Using this as motivation, the total amount of information (both quantum and classical) present in the system was obtained through a unified picture of quantum coherence and correlations in Ref. [27]. This was achieved by defining a new quantity called the hookup M , which is equal to the sum of the mutual information (total correlations) and the local coherence in the system

$$M(\rho) = T(\rho) + C_L(\rho). \quad (\text{A5})$$

Equivalently, it can also be defined as the sum of the total coherence and classical correlations

$$M(\rho) = C(\rho) + K(\rho). \quad (\text{A6})$$

While the above expressions (A5) and (A6) can be used to estimate the total information in the system, it can also be defined using a distance measure as shown in Table I of the main text. We estimate these different correlations for the symmetric $W\bar{W}$ state and the asymmetric star state.

APPENDIX B: QUANTUM STATES

Quantum states with more than two qubits can be entangled in a multitude of different ways (see Fig. 5). It is always convenient to classify them into equivalence classes based on their entanglement structure. There are two methods of classifying entanglement in multipartite systems, one based on stochastic local operations and classical communications (SLOCC) [46] and the other based on local unitary (LU) transformations [60]. In the SLOCC method, multipartite states are divided into different classes based on LOCC transformations. If a group of quantum states can be transformed into one another through LOCC they belong to the same class. For example, based on LOCC, the tripartite quantum states are classified into the GHZ and W classes. The LU decomposition method is based on the entanglement distribution between the different qubits. The pure tripartite states can be classified into six different types based on the LU decomposition method. The classification of quantum correlated states follows the

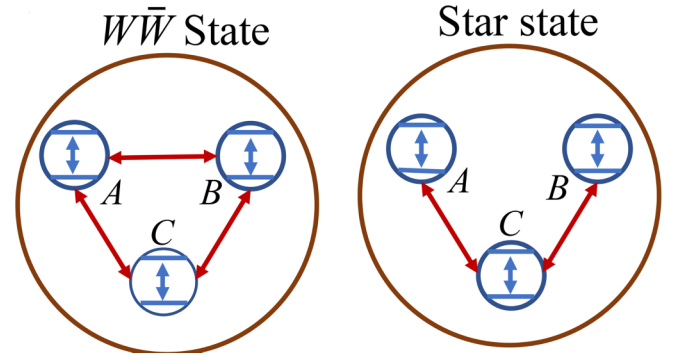


FIG. 6. Schematic sketch of the tripartite $W\bar{W}$ and star states: A , B , and C are the three qubits of the system. The outer circle represents the genuinely tripartite quantum property which is destroyed when a single qubit is lost. Arrows between the qubits denote the quantum property which is distributed in a bipartite fashion. The local coherence due to the superposition of the two levels of the same qubit is shown by the arrows within the qubits. The distribution of the correlations between the qubits on the star state show the asymmetric property of the bipartite correlations.

same pattern as that of entanglement classification using LU decomposition.

In our investigation we consider the $W\bar{W}$ and star states to study the symmetric and asymmetric quantum states. The $W\bar{W}$ state has both bipartite and genuinely tripartite quantum correlations. A quantum correlation is said to be genuinely tripartite when the loss of a single qubit completely destroys it. Similarly, it also has bipartite quantum correlations which are distributed pairwise between all three possible pairs. The coherence in the $W\bar{W}$ state is distributed at all levels and hence it has local coherence, bipartite global coherence, and genuinely tripartite coherence. The $W\bar{W}$ state is said to be symmetric because the reduction in quantum correlation or coherence in the system due to the loss of a qubit does not depend on the label of the qubit which has been traced out. The star state also has both bipartite quantum correlations and genuinely tripartite quantum correlations. In a star state the bipartite correlation is present only between the two pairs of qubits. Hence the star state is asymmetric with respect to the distribution of quantum correlations and coherence. The amount of correlation and coherence left in the system after the loss of a qubit depends on which particular qubit has been removed from the system. An illustrative sketch of the $W\bar{W}$ and star states is given in Fig. 6.

APPENDIX C: EXPERIMENTAL GENERATION OF QUANTUM STATES

A detailed description of the experimental generation of $W\bar{W}$ and star states is given in this Appendix.

1. The $W\bar{W}$ state

A femtosecond pump pulse of central wavelength of 780 nm, pulse duration of 140 fs, and repetition rate of 76 MHz is frequency doubled by a 1.5-mm-thick BBO crystal. To generate a $W\bar{W}$ state, the output ultraviolet pulse is guided to pump a 1-mm-thick beamlike type-II phase-matching BBO

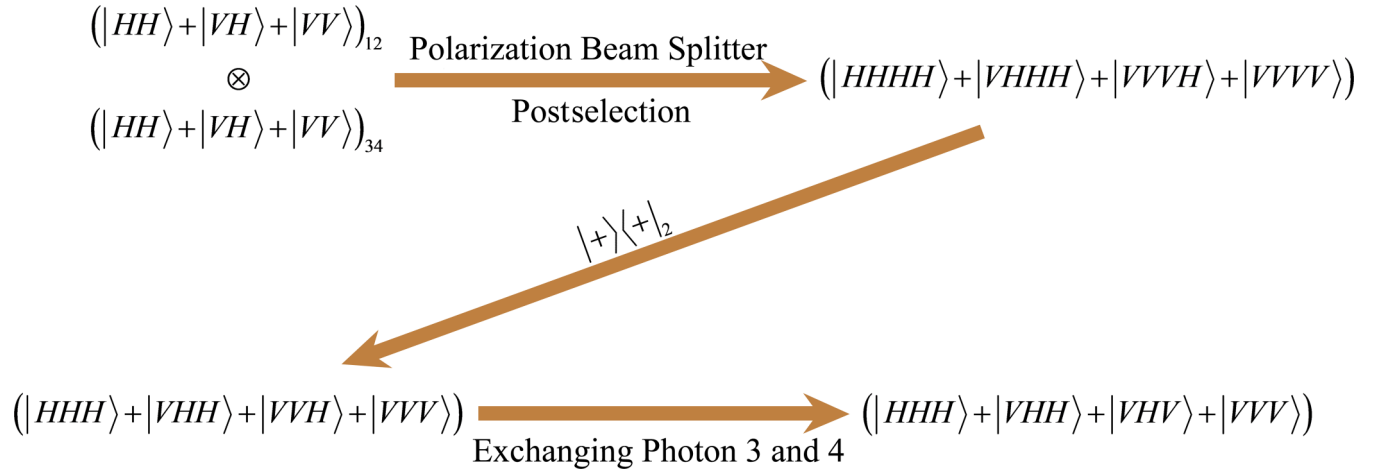


FIG. 7. Diagram of the experimental generation of star states through a step by step process. The preparation method starts with a bipartite quantum system. These states are then subjected to three quantum operations in a succession of steps and the result yields a star state.

crystal. Through SPDC two pairs of down-converted photons are generated. These four photons are overlapped using a PBS. A 3-nm interference filter is used for spectral selection. Using three nonpolarizing beam splitters, the four photons are separated. This process leads to the generation of a four-photon Dicke state with two excitations

$$|D_4^2\rangle = (|HHVV\rangle + |HVHV\rangle + |VHHV\rangle + |HVVH\rangle + |VHVH\rangle + |VVHH\rangle)/\sqrt{6}. \quad (\text{C1})$$

Finally, the $W\bar{W}$ state is generated by projecting one of the qubits into the $(|H\rangle + |V\rangle)/\sqrt{2}$ basis.

2. Star state

The star state is generated using a nonmaximally entangled state $|\psi_1\rangle = (|HH\rangle + |VH\rangle + |VV\rangle)/\sqrt{3}$. By Schmidt decomposition, we can rewrite the state in a new basis $|\psi_1\rangle = \cos\theta|\alpha_1\alpha_2\rangle + \sin\theta|\alpha_1^\perp\alpha_2^\perp\rangle$, with the parameters

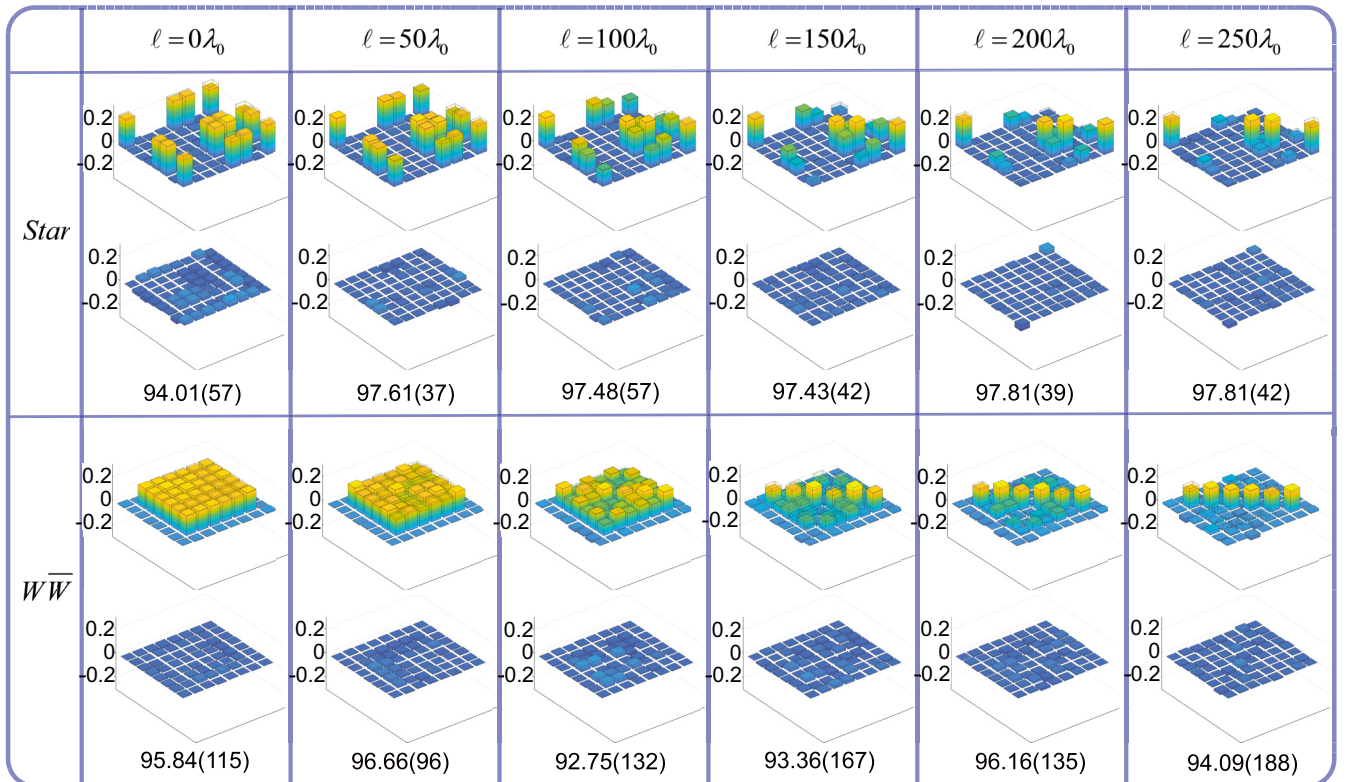


FIG. 8. Reconstruction of the density matrices of the star and $W\bar{W}$ states from the tomography data for three-qubit dephasing. The columns correspond to the dephasing time performed by the quartz plate thickness. In each row the two histograms correspond to the real part (top chart) and the imaginary part (bottom chart) of the density matrix. The theoretical density matrices are shown as transparent histograms. The numerical values of the fidelities of the states in comparison to theory are marked together with error estimates.

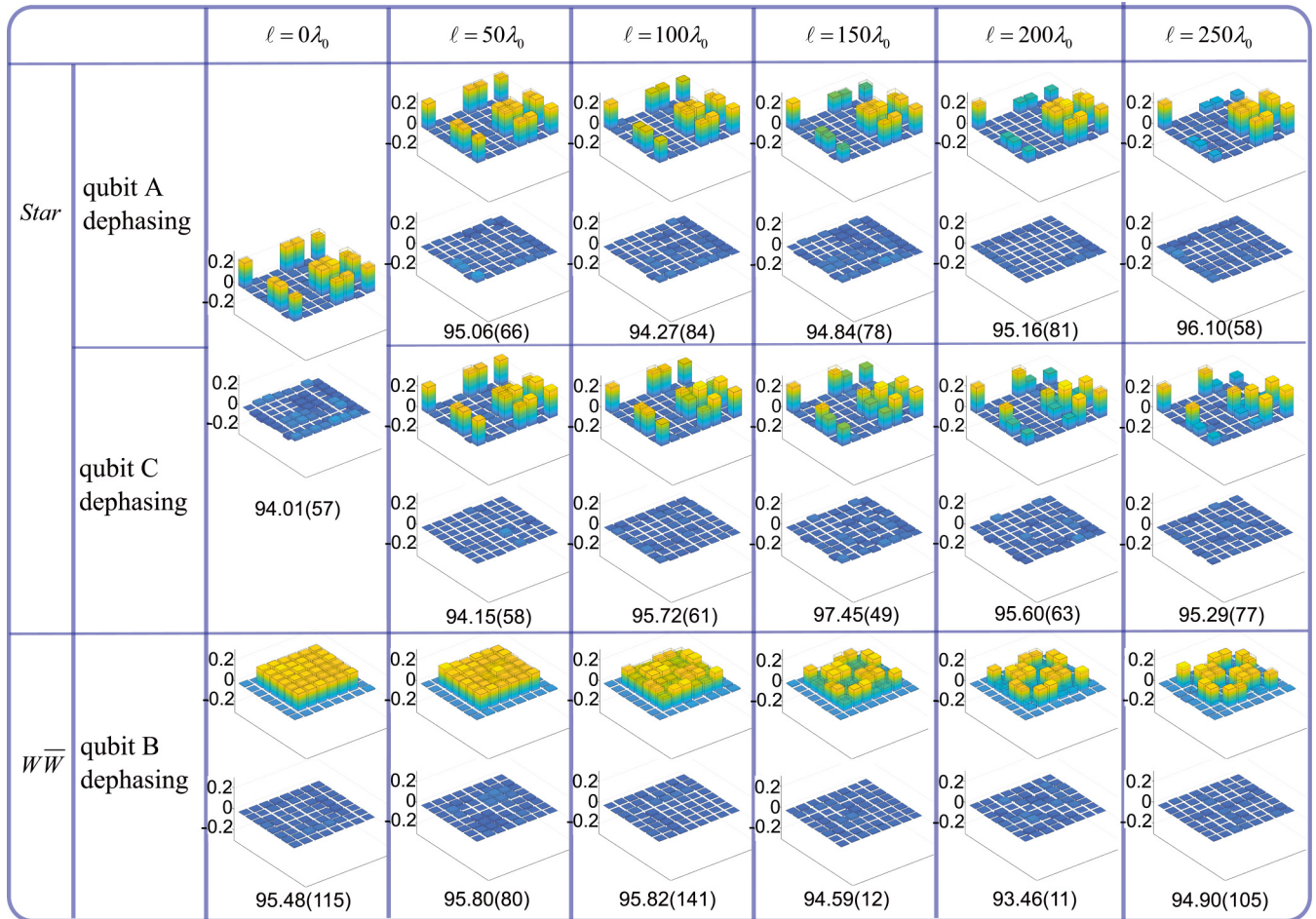


FIG. 9. Reconstruction of the density matrices of the star and $\overline{W\overline{W}}$ states from the tomography data, for single-qubit dephasing. The columns correspond to the dephasing time simulated by the quartz plate thickness. In each row the two histograms correspond to the real part (top chart) and the imaginary part (bottom chart) of the density matrix. The theoretical density matrices are shown as transparent histograms. The numerical values of the fidelities of the states in comparison to theory are marked together with error estimates.

$\cos^2 \theta : \sin^2 \theta = 6.8554$, $|\alpha\rangle = 0.5257|0\rangle + 0.8507|1\rangle$, and $|\alpha^\perp\rangle = 0.8507|0\rangle - 0.5257|1\rangle$.

To generate the nonmaximally entangled state we use a sandwichlike EPR pair source. The setup of this resource consists of a half waveplate sandwiched between 2-mm-thick and 1-mm-thick identical beamlike type-II BBO crystals [49,50]. The first BBO crystal produces the polarization state $|V_{1,o}\rangle|H_{2,e}\rangle$. Here H (V) denotes the horizontal (vertical) polarization, the notation o (e) stands for the ordinary (extraordinary) photons, and 1 and 2 denote the respective emitting paths of the down-converted photons. The half waveplate sandwiched between the two BBO crystals rotates the photonic state to its orthogonal counterpart $|H_{1,o}\rangle|V_{2,e}\rangle$. The second BBO crystal has the same cutting angle as the first and is also placed in the same manner. Hence the second BBO crystal also prepares the photonic state $|V_{1,o}\rangle|H_{2,e}\rangle$. The two possible ways of generating photon pairs (using the first and the second BBO crystal) are made indistinguishable by spatial and temporal compensations due to the birefringent crystals. A LiNbO₃ crystal with a thickness of 4.2 mm (0.5 mm) is used for the temporal

compensation of the extraordinary (ordinary) light. Similarly, a YVO₄ crystal with a thickness of 0.57 mm (0.5 mm) is used for the spatial compensation of the extraordinary (ordinary) light. The spacing between the two BBO crystals can be adjusted to tune the ratio of the photon pairs generated in them.

The multiphoton entangled states are produced using Hong-Ou-Mandel interference. A schematic sketch of the star state production process is given in Fig. 7. In the first step, the two nonmaximally entangled states $|\psi_1\rangle$ from the SPDC source overlaps on a PBS for interference. The PBS acts as a parity check gate $|HH\rangle\langle HH| + |VV\rangle\langle VV|$ on the two interfering photons where there is one and only one photon in each output port. After this process we have a four-qubit quantum state. In the output state of the first step, the second photon is projected onto $|+\rangle = (|H\rangle + |V\rangle)/\sqrt{2}$. Due to this projective measurement, the four-qubit quantum state is reduced to a three-qubit quantum state. Here we would like to note that there is no relabeling to quantum states after the projective measurement. Finally, qubits 3 and 4 are exchanged to obtain the star states.

APPENDIX D: DEPHASING CHANNEL DUE TO THE BIREFRINGENT CRYSTAL

A polarized photon gets dephased on passing through a birefringent crystal. This can be used to controllably simulate the decoherence due to dephasing in a linear optical system. The down-converted (SPDC) photons have a frequency distribution which approximates to a Gaussian function [61]. Under this spectral condition, the action of a quartz plate on an initial qubit state $|\psi_0\rangle = \alpha|0\rangle + \beta|1\rangle$ is described as

$$\varepsilon_\ell(\rho) = \begin{bmatrix} |\alpha|^2 & \alpha\beta^*\mathcal{F}(\ell) \\ \alpha^*\beta\mathcal{F}^*(\ell) & |\beta|^2 \end{bmatrix}.$$

Here ℓ represents the effective path difference which is proportional to the thickness of the quartz plate. The coherence behavior functional is exponential by nature and reads $\mathcal{F}(\ell) = \exp(-\Gamma\ell^2)$, where Γ is the decay rate. To find the decay rate Γ , we fit the single-photon coherence behavior $\mathcal{F}(\ell)$ under decoherence. The decay rate Γ for the $W\bar{W}$ state is measured to be $\Gamma = 2.2083 \times 10^{-5}\lambda_0^{-2}$ with a 3-nm interference filter for each particle. For the star state $\Gamma = 2.0624 \times 10^{-5}\lambda_0^{-2}$ while using a 2-nm interference filter for each particle. The action of a quartz plate on a quantum state is equivalent to a

phase flip map $\varepsilon_\ell(\rho) = [1 - p(\ell)]\rho + p(\ell)\sigma_z\rho\sigma_z$, where $p(\ell)$ is the mixing probability and σ_z is the Pauli spin matrix. This action can be decomposed in two Kraus operators

$$M_0 = \sqrt{1 - p(\ell)}\mathcal{I}, \quad M_1 = \sqrt{p(\ell)}\sigma_z, \quad (\text{D1})$$

where $p(\ell) = [1 - \exp(-\Gamma\ell^2)]/2$. Using (D1), we can describe the tripartite system in a dephasing environment as

$$\varepsilon_\ell^{\otimes 3}(\rho_{123}) = \sum_{i,j,k=0}^1 M_i^\dagger \otimes M_j^\dagger \otimes M_k^\dagger \rho_{123} M_i \otimes M_j \otimes M_k. \quad (\text{D2})$$

The experimental density matrices at various stages of the dephasing dynamics are reconstructed using tomography. The experimental tomographic density matrix and the theoretical predictions for various values of path difference are given in Figs. 8 and 9. The theoretical predictions are also shown in Figs. 8 and 9 for the sake of comparison. The expression in (D2) describes a three-channel dephasing. To describe a single-channel dephasing, we will use the Kraus operator corresponding to only one qubit and the other two qubits will be subjected to an identity operation. In our work we look into both three-channel and single-channel dephasing of the $W\bar{W}$ and star states.

[1] A. Steane, *Rep. Prog. Phys.* **61**, 117 (1998).
 [2] J. P. Dowling and G. J. Milburn, *Philos. Trans. R. Soc. A* **361**, 1655 (2003).
 [3] T. D. Ladd, F. Jelezko, R. Laflamme, Y. Nakamura, C. Monroe, and J. L. O’Brien, *Nature (London)* **464**, 45 (2010).
 [4] H.-P. Breuer and F. Petruccione, *The Theory of Open Quantum Systems* (Oxford University Press, Oxford, 2002).
 [5] W. H. Zurek, *Rev. Mod. Phys.* **75**, 715 (2003).
 [6] F. Fröwis, P. Sekatski, W. Dür, N. Gisin, and N. Sangouard, *Rev. Mod. Phys.* **90**, 025004 (2018).
 [7] T. Yu and J. H. Eberly, *Phys. Rev. B* **66**, 193306 (2002).
 [8] A. Shimizu and T. Miyadera, *Phys. Rev. Lett.* **89**, 270403 (2002).
 [9] D. Janzing and T. Beth, *Phys. Rev. A* **61**, 052308 (2000).
 [10] F. Fröwis and W. Dür, *New J. Phys.* **14**, 093039 (2012).
 [11] W. Dür, C. Simon, and J. I. Cirac, *Phys. Rev. Lett.* **89**, 210402 (2002).
 [12] A. N. Boto, P. Kok, D. S. Abrams, S. L. Braunstein, C. P. Williams, and J. P. Dowling, *Phys. Rev. Lett.* **85**, 2733 (2000).
 [13] J. P. Dowling, *Contemp. Phys.* **49**, 125 (2008).
 [14] V. Giovannetti, S. Lloyd, and L. Maccone, *Nat. Photon.* **5**, 222 (2011).
 [15] J. S. Bell, *Phys. Phys. Fiz.* **1**, 195 (1964).
 [16] A. Einstein, B. Podolsky, and N. Rosen, *Phys. Rev.* **47**, 777 (1935).
 [17] H. M. Wiseman, S. J. Jones, and A. C. Doherty, *Phys. Rev. Lett.* **98**, 140402 (2007).
 [18] R. Horodecki, P. Horodecki, M. Horodecki, and K. Horodecki, *Rev. Mod. Phys.* **81**, 865 (2009).
 [19] H. Ollivier and W. H. Zurek, *Phys. Rev. Lett.* **88**, 017901 (2001).
 [20] L. Henderson and V. Vedral, *J. Phys. A: Math. Gen.* **34**, 6899 (2001).
 [21] T. Baumgratz, M. Cramer, and M. B. Plenio, *Phys. Rev. Lett.* **113**, 140401 (2014).
 [22] C. Radhakrishnan, M. Parthasarathy, S. Jambulingam, and T. Byrnes, *Phys. Rev. Lett.* **116**, 150504 (2016).
 [23] K. C. Tan, H. Kwon, C.-Y. Park, and H. Jeong, *Phys. Rev. A* **94**, 022329 (2016).
 [24] G. Adesso, T. R. Bromley, and M. Cianciaruso, *J. Phys. A: Math. Theor.* **49**, 473001 (2016).
 [25] Z.-H. Ma, J. Cui, Z. Cao, S.-M. Fei, V. Vedral, T. Byrnes, and C. Radhakrishnan, *Europhys. Lett.* **125**, 50005 (2019).
 [26] K. Modi, T. Paterek, W. Son, V. Vedral, and M. Williamson, *Phys. Rev. Lett.* **104**, 080501 (2010).
 [27] F. Galve, G. L. Giorgi, and R. Zambrini, in *Lectures on General Quantum Correlations and their Application*, edited by F. F. Fanchini, D. d. O. Soares Pinto, and G. Adesso, Quantum Science and Technology (Springer International, Cham, 2017), pp. 393–420.
 [28] E. Chitambar and G. Gour, *Rev. Mod. Phys.* **91**, 025001 (2019).
 [29] A. Winter and D. Yang, *Phys. Rev. Lett.* **116**, 120404 (2016).
 [30] F. G. S. L. Brandão and G. Gour, *Phys. Rev. Lett.* **115**, 070503 (2015).
 [31] C. Radhakrishnan, I. Ermakov, and T. Byrnes, *Phys. Rev. A* **96**, 012341 (2017).
 [32] E. Chitambar and M.-H. Hsieh, *Phys. Rev. Lett.* **117**, 020402 (2016).
 [33] M. Horodecki and J. Oppenheim, *Int. J. Mod. Phys. B* **27**, 1345019 (2013).
 [34] E. Chitambar and G. Gour, *Phys. Rev. Lett.* **117**, 030401 (2016).
 [35] J.-S. Xu, C.-F. Li, M. Gong, X.-B. Zou, C.-H. Shi, G. Chen, and G.-C. Guo, *Phys. Rev. Lett.* **104**, 100502 (2010).
 [36] J.-S. Xu, X.-Y. Xu, C.-F. Li, C.-J. Zhang, X.-B. Zou, and G.-C. Guo, *Nat. Commun.* **1**, 7 (2010).

- [37] J.-S. Xu, K. Sun, C.-F. Li, X.-Y. Xu, G.-C. Guo, E. Andersson, R. L. Franco, and G. Compagno, *Nat. Commun.* **4**, 2851 (2013).
- [38] N. K. Bernardes, A. Cuevas, A. Orioux, C. Monken, P. Mataloni, F. Sciarrino, and M. F. Santos, *Sci. Rep.* **5**, 17520 (2015).
- [39] B. Bellomo, R. Lo Franco, and G. Compagno, *Phys. Rev. Lett.* **99**, 160502 (2007).
- [40] J. H. Eberly and T. Yu, *Science* **316**, 555 (2007).
- [41] C. E. López, G. Romero, F. Lastra, E. Solano, and J. C. Retamal, *Phys. Rev. Lett.* **101**, 080503 (2008).
- [42] T. Yu and J. H. Eberly, *Science* **323**, 598 (2009).
- [43] L. Mazzola, J. Piilo, and S. Maniscalco, *Phys. Rev. Lett.* **104**, 200401 (2010).
- [44] T. Werlang, S. Souza, F. F. Fanchini, and C. J. Villas Boas, *Phys. Rev. A* **80**, 024103 (2009).
- [45] J. Maziero, L. C. Céleri, R. M. Serra, and V. Vedral, *Phys. Rev. A* **80**, 044102 (2009).
- [46] W. Dür, G. Vidal, and J. I. Cirac, *Phys. Rev. A* **62**, 062314 (2000).
- [47] M. Plesch and V. Bužek, *Phys. Rev. A* **67**, 012322 (2003).
- [48] S. Anders and H. J. Briegel, *Phys. Rev. A* **73**, 022334 (2006).
- [49] C. Zhang, Y.-F. Huang, Z. Wang, B.-H. Liu, C.-F. Li, and G.-C. Guo, *Phys. Rev. Lett.* **115**, 260402 (2015).
- [50] X.-L. Wang, L.-K. Chen, W. Li, H.-L. Huang, C. Liu, C. Chen, Y.-H. Luo, Z.-E. Su, D. Wu, Z.-D. Li, *et al.*, *Phys. Rev. Lett.* **117**, 210502 (2016).
- [51] V. Vedral, *Rev. Mod. Phys.* **74**, 197 (2002).
- [52] V. Vedral, M. B. Plenio, M. A. Rippin, and P. L. Knight, *Phys. Rev. Lett.* **78**, 2275 (1997).
- [53] V. Vedral and M. B. Plenio, *Phys. Rev. A* **57**, 1619 (1998).
- [54] C. Radhakrishnan, P.-W. Chen, S. Jambulingam, T. Byrnes, and M. M. Ali, *Sci. Rep.* **9**, 2363 (2019).
- [55] K.-D. Wu, Z. Hou, Y.-Y. Zhao, G.-Y. Xiang, C.-F. Li, G.-C. Guo, J. Ma, Q.-Y. He, J. Thompson, and M. Gu, *Phys. Rev. Lett.* **121**, 050401 (2018).
- [56] J. Maziero, T. Werlang, F. F. Fanchini, L. C. Céleri, and R. M. Serra, *Phys. Rev. A* **81**, 022116 (2010).
- [57] C. Radhakrishnan, M. Lauriere, and T. Byrnes, *Phys. Rev. Lett.* **124**, 110401 (2020).
- [58] C. Radhakrishnan, Z. Ding, F. Shi, J. Du, and T. Byrnes, *Ann. Phys. (NY)* **409**, 167906 (2019).
- [59] A. Streltsov, U. Singh, H. S. Dhar, M. N. Bera, and G. Adesso, *Phys. Rev. Lett.* **115**, 020403 (2015).
- [60] A. Acín, A. Andrianov, L. Costa, E. Jané, J. I. Latorre, and R. Tarrach, *Phys. Rev. Lett.* **85**, 1560 (2000).
- [61] W. P. Grice, A. B. U'Ren, and I. A. Walmsley, *Phys. Rev. A* **64**, 063815 (2001).